



ZnO nanostructure synthesis for the photocatalytic degradation of azo dye methyl orange from aqueous solutions utilizing activated carbon

Ahmed Jaber Ibrahim ^{a,*}

^aScientific Research Center, Al-Ayen University, ThiQar 64011, Iraq

ARTICLE INFO:

Received 3 Sep 2022

Revised form 29 Oct 2022

Accepted 18 Nov 2022

Available online 29 Dec 2022

Keywords:

Degradation,
Zinc oxide,
Nanostructure,
Methyl orange,
Photocatalytic

ABSTRACT

In this study, zinc acetate (as a precursor) and activated carbon carboxylic acid derivative were used to create the nanostructure of zinc oxide (ZnO) as a matrix. The carboxylic acid derivative was produced by modifying the oxidized activated carbon with nitric acid (AC-COOH). The modified activated carbon's surface was then impregnated with zinc to load it. By using BET, XRD, and SEM to characterize the ZnO nanostructure, it was discovered that it was composed of nanoparticles with a surface area capacity of 17.78 m² g⁻¹ and a size range of 21–31 nm. The photocatalytic hydrolysis of the dye methyl orange in an aqueous medium served as a test case for the catalyst's performance. The primary variables were considered, including pH, catalyst dose, stirring effect, and starting dye concentration. Measurements of activity below UV light revealed satisfactory outcomes for photocatalytic hydrolysis of the methyl orange (MO). In addition, the efficiency of the methyl orange (MO) photolysis catalyst prepared with unmodified activated carbon was also evaluated. The outcomes proved that zinc oxide (ZnO), made using a derivative carboxylic acid of activated carbon molecules by a matrix, had more good photocatalytic action than zinc oxide (ZnO) made by the real activated carbon matrix.

1. Introduction

Reactive dye-containing effluents from various sectors frequently generate environmental issues [1]. The ecosystem of the receiving surface waterways is severely harmed by this pollution [2]. Many researchers' efforts have focused on removing pollutants and toxins from wastewater from different sectors [3]. A variety of chemical and physical procedures, such as membranes [4], adsorption methods [5], and photolysis, have been employed to remove dyes [6] presently. Several researchers

have recently used photolysis as one of the advanced oxidation processes (AOPs) to get rid of dyes from wastewater [7]. Without altering the substrate, the photocatalytic reaction is catalyzed by light and can proceed more quickly [8]. Under the right circumstances, semiconductors function as catalysts due to the down breaking energy between the capacitance and conduction bands [9]. The process of photocatalysis requires two levels of different, equal energy. The movement of the electrons caused by the absorption of this energy leads to a hole (h⁺) and a pair of electrons(e⁻). Both the oxidation of the electron donor species and the reduction of the electron acceptor species might include electrons [10]. To degrade pollutants, many materials are

*Corresponding Author: Ahmed Jaber Ibrahim

Email: ahmed.jibrahim@alayen.edu.iq

<https://doi.org/10.24200/amecj.v5.i04.200>

utilized as photocatalysts, including TiO_2 , ZnO , ZrO_2 , CdS , MoS_2 , and WO_3 [11]. TiO_2 is one of these materials frequently used as a photocatalyst and has seen the most application to date. TiO_2 has benefits like environmental safety, non-toxicities, chemical constancy, and the capacity for restoration and reuse. However, TiO_2 has drawbacks, including a high price tag and a UV absorption band. The importance of ZnO as a suitable TiO_2 alternative in photocatalysis has lately increased [12]. One richest structures, zinc oxide, has a variety of advantages. As a result, ZnO has several uses in various scientific projects [13]. ZnO has been produced using a variety of techniques, including the soft chemical method [14], the sol-gel method [15], the vapor-phase growth [16], the vapor-liquid-solid process [17], electrophoretic deposition [18], thermal evaporation [19], homogeneous precipitation [20], chemical vapor deposition [21], chemical bath deposition [22], etc. In the aforementioned investigations, ZnO nanoparticles were only occasionally generated through the activated carbon layer and by an auxiliary matrix approach, as recommended by Park et al. [23]. In this study, the photocatalytic activity of the generated ZnO was used to break down the azo dye methyl orange. Additionally, ZnO was produced using modified activated carbon (containing carboxyl functional groups).

2. Materials and Methods

2.1. Reagents

All chemical substances were obtained with a high degree of purity, including caustic soda (NaOH , CAS Number: 1310-73-2, Sigma), hydrochloric acid (HCl , CAS Number: 7647-01-0, Sigma, Germany), activated carbon (AC, CAS Number: 7440-44-0, Sigma), zinc acetate dihydrate ($\text{Zn}(\text{CH}_3\text{CO}_2)_2 \cdot 2\text{H}_2\text{O}$, CAS Number: 5970-45-6, Sigma), nitric acid (HNO_3 , CAS Number: 7697-37-2, Sigma, Germany), and azo dye methyl orange ($\text{C}_{14}\text{H}_{14}\text{N}_3\text{O}_3\text{SNa}$, CAS Number: 547-58-0, Sigma). Methyl orange was dissolved in 100 mL of deionized water (DI), 0.010 g at a time, to create a stock solution (100 g mL^{-1}). All working solutions were made at the necessary concentration using distilled water to dilute the stock solution.

2.2. Equipment

An ultraviolet-visible spectrophotometer (model 2600) to record Rayleigh UV-Vis spectra. A Metrohm pH meter (model 744) to adjust the working solution's pH to the desired values. Field emission-scanning electron microscope (FE-SEM) (model SU5000) to know the characterization of the sample's surface and shape morphology. X-ray diffraction instrument (XRD) (model B8 ADVANCE) to record patterns via BRUKER. The transformer coupled plasma (TCP) (model VISTA-PRO) to measure the presence of zinc in the samples. Spectrophotometer (IR-470 Shimadzu) to record the Infrared (IR) spectrum of samples. At the analytical chemistry laboratory of the college of education (Ibn Al-Haitham) at the University of Baghdad, experiments in the photocatalytic bleaching and degradation of dye MO were carried out at a photoreactor framework prepared there for it.

2.3. Synthesizing Zinc Oxide nanoparticles by modified activated carbon particles

2.3.1. Activated carbon surface modification

According to Chang et al. [24], adding carboxyl functional groups to the surface of activated carbon caused the carbon particles to become activated. To eliminate metal ions and other impurities, a hydrochloric solution (10% v/v) solution was first used to clean the activated carbon powder for 24 hours. Following that, 300 ml of a 32.5 % (v/v) HNO_3 solution was stirred with 10 g of pure activated carbon added, and the mixture was heated at $60 \text{ }^\circ\text{C}$ for five hours. The heterogeneous mixture had filtered and neutralized with DI water (deionized water) by wash and then dried below decreased pressure for eight hours at $80 \text{ }^\circ\text{C}$. the carboxylic derivative of activated carbon makes up the final product (AC-COOH).

2.3.2. Synthesizing nanoparticles of zinc oxide

As a precursor for manufacturing ZnO nanoparticles, 100 mL of zinc acetate solution was mixed with 2 g of carboxylate-activated carbon (AC-COOH) in different concentrations for 12 hours. The solution was filtered, dried for 18 hours at $80 \text{ }^\circ\text{C}$, and then

calcined for 4 hours at 500 °C in an electric oven. Different concentrations of zinc acetate dihydrate were explored to create zinc nanoparticles by examining the impact of the concentration of zinc acetate precursor on the description of zinc oxide (particle size, percentage values, photocatalytic capabilities, etc.). To do this, ZnO nanoparticles were created using solutions containing concentrations of 0.09, 0.02, and 0.01 M (Molarity) zinc acetate dihydrate, respectively. XRD spectra of three samples were taken to verify the production of ZnO nanoparticle forms. The XRD bandwidth pattern and Scherrer's Equation 1 [25, 26] were used to measure the crystal size of three samples.

$$D = K (\lambda / \beta \cos \theta) \quad (\text{Eq.1})$$

Where D represents the size of crystalline particle in units of a nanometer (nm), The coefficient is K (that equals 0.89), λ represents the wavelength of the X-ray radiation in a unit of a nanometer (nm), β means FWHM (full width at half maximum) is an experimental value in radians (rad) and diffraction angle expressed in degrees had represented θ .

2.3.3. Synthesis of Zinc Oxide nanoparticles utilizing unmodified activated carbon

2.0 g of activated carbon had put in 200 mL of hydrochloric solution (10% v/v) to eliminate impurities for twenty-four hours to study the surface modification phase of activated carbon particles in the formation of Zinc Oxide (ZnO). After that, the product was added to a concentration of 0.09 M zinc acetate dihydrate solution for 12 hours, and the resulting combination was then filtered. The finished product was dried at 80 °C for 18 hours before being calcined in an electric oven for 4 hours at 500 °C. To determine the sample's crystal size using Scherrer's equation, XRD spectra were taken on a sample made with unmodified activated carbon.

2.4. Procedure of methyl orange decomposition in photocatalytic experiments

Initially, a 250 mL beaker was filled with 100 mL of methyl orange (MO) solution with a concentration

of 10 mg L⁻¹ and a pH of 6. The solution was then supplemented with 20 mg of Zinc Oxide (ZnO) photocatalyst. Methyl orange was adsorbed onto Zinc Oxide (ZnO) nanoparticles after being combined with the solution utilizing a magnetic stirring device in a dark environment for half hour (30 min). Afterward confirming the balance of adsorption, 0.2 mL of the solution was placed into a test tube and then centrifuged for five minutes at 3000 rpm to collect the photocatalyst deposition particles. A spectrophotometer captured the solution's adsorption spectra in the 200–600 nm range. After the absorption spectrum was recorded, the combination was put into a photoreactor, and a UV light was turned on. Twenty minutes after exposure to UV light, ten samples were collected at intervals of one, and their absorption spectra were recorded. The control solution's adsorption spectrum was recorded similarly without including a photocatalyst.

2.5. Procedure of batch adsorption

To find the best circumstances for bleaching and degrading MO (methyl orange) in the existence of Zinc Oxide (ZnO) photocatalysts, batch experiments were carried out. It was thoroughly explored how relevant factors including methyl orange (MO) concentration, pH, solution stirring, photocatalyst dose, and solution oxygen affected the outcomes. One variable at a time optimization was utilized to improve factors that affected the reaction. With this procedure, studies were carried out in a batch setting with 100 mL of dye solution (10 mg L⁻¹) placed into a beaker (250 ml). The magnetic stirrer was used to mix the suspensions for 30 minutes in the dark before centrifuging them for 5 minutes at 3000 rpm. A UV-Vis spectrophotometer was used to evaluate the clear supernatant. Equation (2) was used to determine the rate of bleaching and dye degradation [27].

$$R = (C_0 - C_t \div C_0) \times 100 \quad (\text{Eq. 2})$$

Where R (percentage) represents the dye removal effectiveness, C_0 represents the dye's starting concentration (mg L⁻¹), and C_t represents the dye's concentration at time t following adsorption (mg L⁻¹).

3. Results and Discussion

3.1. Study of Nanoparticles' characteristics

3.1.1. X-Ray Diffraction (XRD) examination

The XRD spectra of three produced zinc oxide (ZnO) samples are shown in Figure 1 to illustrate that the nanoparticles formed appropriately. Figures 1 show that the sample's hexagonal zinc

oxide crystallization has been verified. Table 1 compares the XRD pattern characteristics for three produced samples and the reference sample [22]. It can be seen from the XRD spectrum in Figure 1 and the data in Table 1 that as zinc acetate dihydrate concentration increased, ZnO peak density too increased, and spectral noise intensity

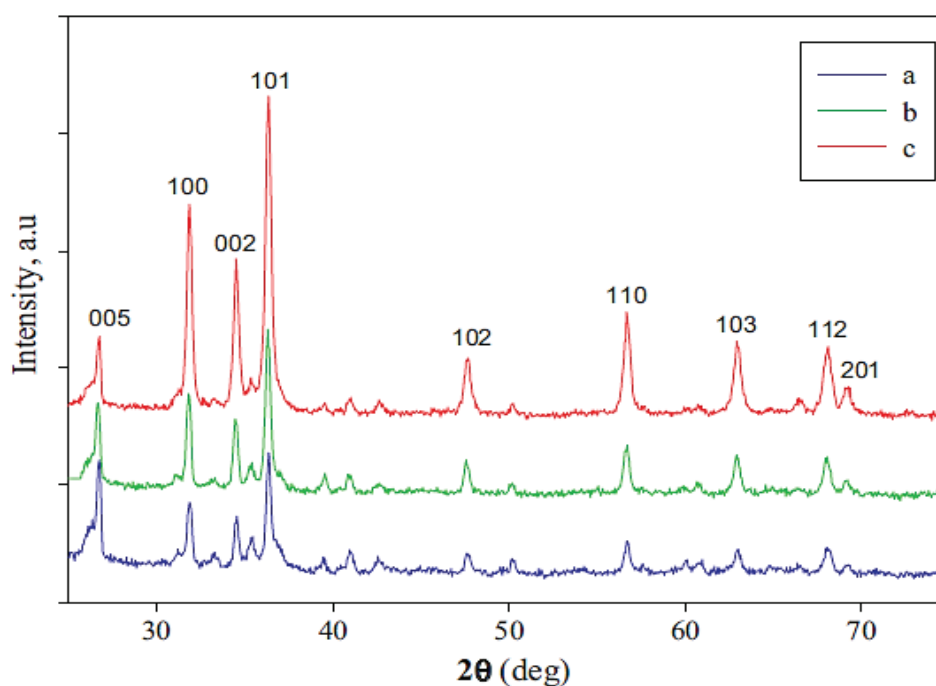


Fig. 1. XRD spectra of synthetic ZnO nanoparticles at various concentrations of zinc acetate dihydrate (a:0.01 M; b: 0.02 M; c: 0.09 M)

Table 1. Compares the standard sample with the XRD samples (a), (b), and (c), as well as a sample made with unmodified carbon

Standard sample		Samples						the sample produced utilizing unmodified carbon		
		A		b		C				
<u>hkl</u>	d (Å)	I/I ⁰	d (Å)	I/I ⁰						
100	2.82	58	2.81	68	2.82	67	2.81	69	2.75	32
002	2.61	45	2.60	86	2.60	55	2.60	53	2.52	91
101	2.48	100	2.47	100	2.48	100	2.48	100	2.32	100
110	1.63	33	1.63	42	1.63	40	1.63	37	1.51	33

d angstrom distance(Å) between plates, I peak intensity, I⁰ maximum intensity to planes 100 and 002, 101 and 110

decreased. This data may result from increased ZnO nanostructure production with rising zinc acetate concentration. This data may be the result of increased ZnO nanostructure production with rising zinc acetate concentration. According to Liu et al. [20], the intensity of peak 005 in XRD spectra is associated with carbon impurities that became less intense as zinc acetate dihydrate concentration

was raised. Figure 2 displays the XRD spectrum of the carbon-free synthetic sample. The production of hexagonal ZnO has been confirmed based on Table 1 and the differentiation of the XRD data of the produced samples (unmodified activated carbon and the standard sample). Three samples that were created using both modified and unmodified carbon are shown in Table 2 by their crystal sizes.

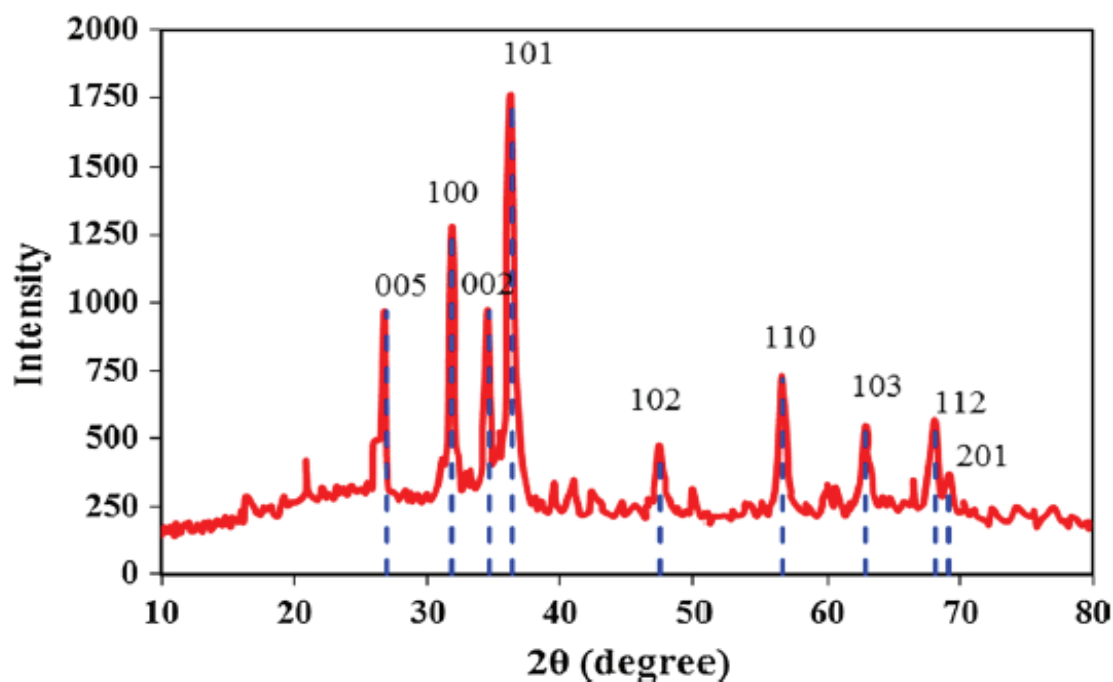


Fig. 2. XRD spectra sample using unmodified carbon and 0.09 M of zinc acetate dihydrate.

Table 2. Scherrer's equation-derived estimated particle size

Planes	Sample size (nm)			the sample produced utilizing unmodified carbon
	A	b	C	
101	26	25	22	24.50
100	27	28	24	36.66
002	33	27	25	25.34

3.1.2. Study analysis using TCP, BET, and SEM

The ZnO percent (%) in samples was calculated using TCP analysis. ZnO content was 9.94, 10.74, and 31.81 % in samples a, b, and c, respectively, according to TCP analysis. These findings suggest that raising the zinc acetate concentration leads to an increase in the samples' ZnO content. ZnO percent was 19.8% for unmodified carbon in the TCP measurement, demonstrating that ZnO % is decreased in the absence of surface modification of activated carbon. The specific surface area of produced ZnO nanoparticles was measured using BET analysis (only for sample c). The specific surface area of this material is higher than the specific surface area of traditional ZnO particles ($4.49 \text{ m}^2 \text{ g}^{-1}$), according to the results of the BET study, which also revealed a total pore volume of $0.1 \text{ cm}^3 \text{ g}^{-1}$ and average pore width of 51.6 nm [28]. The inclusion of activated carbon in the produced ZnO accounts for this elevated amount. ZnO, activated carbon, and AC-ZnO surface morphology and textural characterization are significant criteria that could improve the efficiency of the photocatalytic activity [29]. SEM images of samples a, b, and c as shown in Figure 3, were taken to evaluate the morphology feature of produced ZnO nanoparticles. It is evident that when the concentration of zinc acetate rises, ZnO particles fill the pores of the activated carbon, achieving uniform coverage on a large portion of the activated carbons. Even though

the large holes in the activated carbon were filled with ZnO particles, which prevent the porosity of the carbon surface, sample C nevertheless displays a porous nature with a sizable amount of surface area and pore volume [30].

3.2. Study Ultraviolet-Visible (UV-Vis) spectroscopic examination

Two adsorption bands at wavelengths of 464 and 272 nm can be seen in the methyl orange adsorption spectra. While the breakdown of the azo link, which results in bleaching, causes the absorption band at 464 nm to drop, the methyl orange absorption band decreases at 272 nm due to the phenyl rings degrading and completing mineralization. As seen in Figure 4, decolorization rates are very low, and there is no total degradation or mineralization when ZnO photocatalyst is not present. In contrast to what is depicted in Figure 5, complete bleaching and degradation take place when ZnO nanoparticles are present as a catalyst. For additional research, Figure 6 shows the absorption trend over time at wavelengths of 464 nm and 272 nm under three different circumstances: Ultraviolet radiation, dark medium, and ultraviolet radiation with the catalyst present.

The following figure demonstrates that dye methyl orange completely bleaches and degrades in the presence of a ZnO catalyst within 200 minutes; still, these processes were nonexistent in the absence of

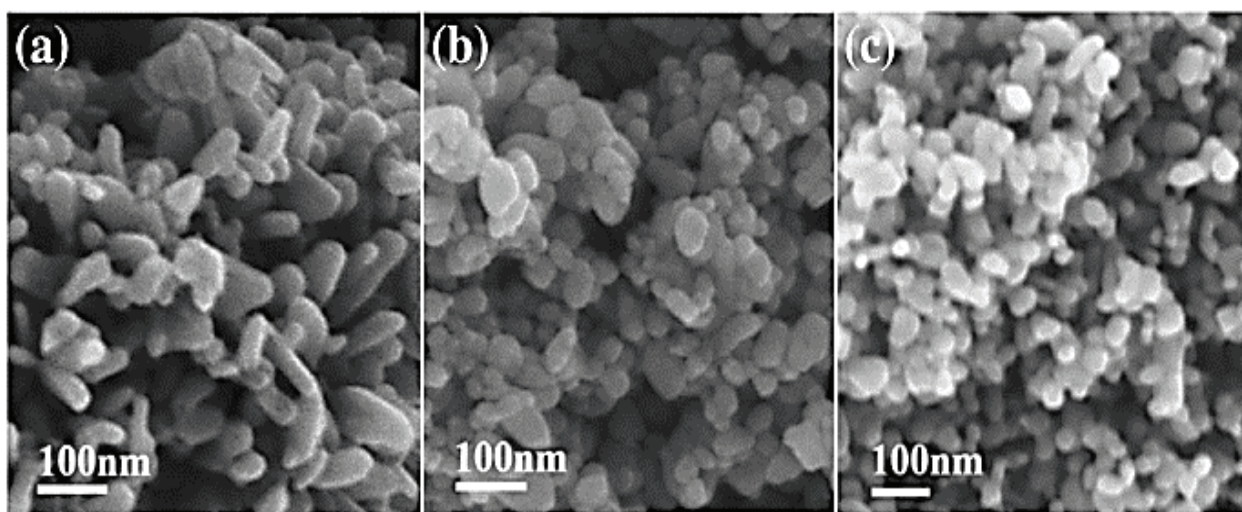


Fig. 3. SEM characterization for three samples (a, b, and c)

a photocatalyst. After swirling the dye and catalyst combination in the dark for 20 minutes, data analysis revealed that no simple degradation occurred and that the adsorption of dye methyl orange onto the

surface catalyst was stable. As a result, dye and catalyst mixtures were swirled for 30 minutes in complete darkness in each experiment to guarantee that adsorption equilibrium was reached.

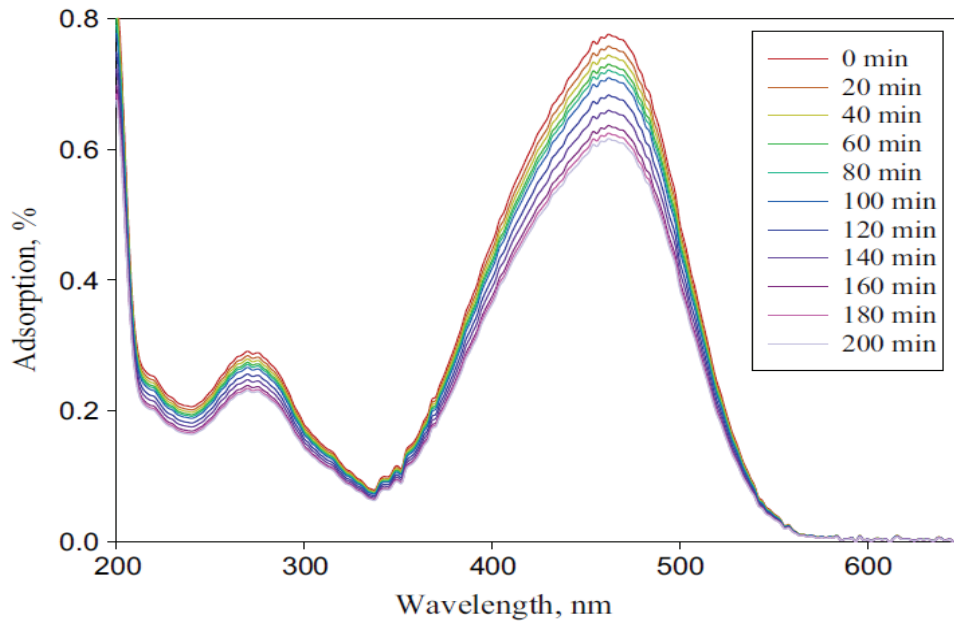


Fig. 4. Shows the reaction system's adsorption spectrum without a ZnO photocatalyst, with 10 mg L^{-1} of methyl orange as the catalyst.

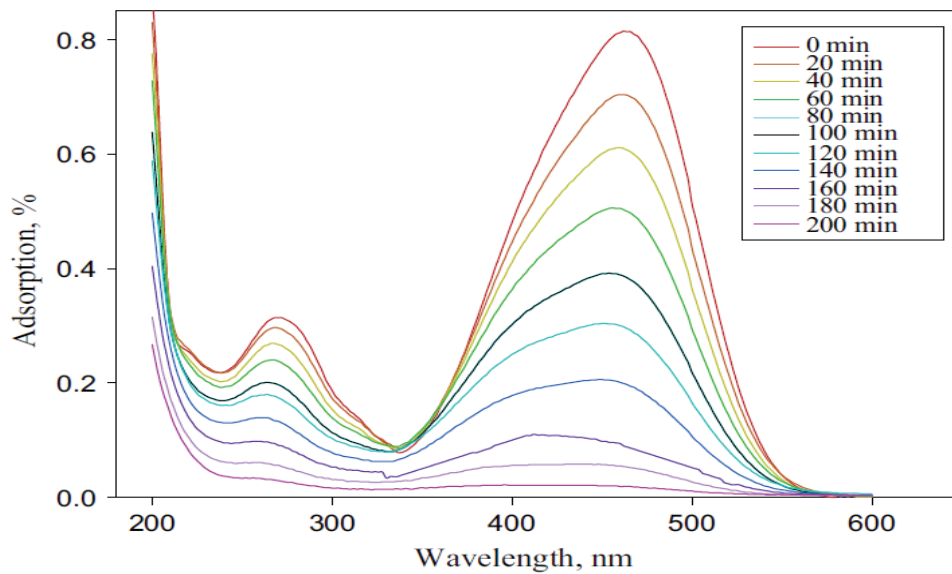


Fig. 5. Shows the reaction system's adsorption spectrum at pH 6, 200 mg L^{-1} of ZnO photocatalyst, and 10 mg L^{-1} of methyl orange.

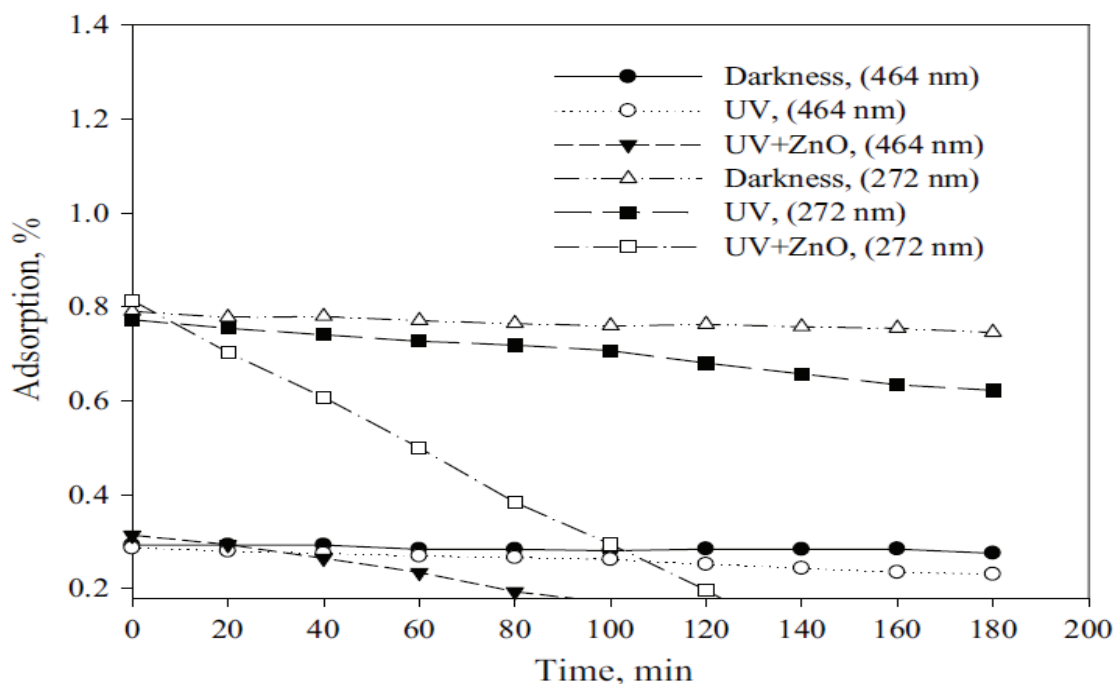


Fig. 6. The light absorption at wavelengths of 272 and 464 nm changes over time under the conditions at pH 6, 200 mg L⁻¹ of photocatalyst, and 10 mg L⁻¹ of methyl orange.

3.3. pH effect

The pH significantly affects the adsorption capacity of the adsorbent and removal efficiency by changing the adsorption chemistry of the adsorbent-adsorbate [31]. The appropriate contact time was used to dissolve 20 mg of photocatalyst into 100 mL of MO solution (10 mg L⁻¹) for the pH-related experiments. To change the pH of the solution, 0.1 M HCl and 0.1 M NaOH solution were utilized. Figure 7 shows how the pH of the solution affects how quickly MO is bleached and degraded by AC-ZnO. It is clear that pH six results in the fastest bleaching and dye degradation of methyl orange (MO). Therefore, pH six was chosen for additional research. Changes in the electrostatic attraction between the dye MO and the ZnO surface can explain this removal process's pH-dependent behavior. In comparison to acidic circumstances (where the driving force is higher), the pollutant

adheres to the adsorbent particles more effectively under optimal electrostatic attraction [32]. ZnO's surface charge is positive at low pH 9 [33]. As a result, anions are more likely to bind to ZnO in an aqueous environment at a low pH of 9. However, the pKa for methyl orange has been reported to be 3.8 ± 0.02 [34]. As a result, at pH values higher than pKa, the concentration of methyl orange in its anionic form is greater than in its cationic form. The amount of methyl orange that could be adsorbed onto ZnO increased as the solution pH was raised to 6. The rate of bleaching and dye degradation was shown to decrease at increasing pH values above 6, because the hydroxyl radical's oxidation potential decreases with the rising pH of the solution [35]. Additionally, the anionic form of methyl orange competes with OH ions in the solution due to the greater OH content, which lowers the capacity of methyl orange to bind to ZnO [36].

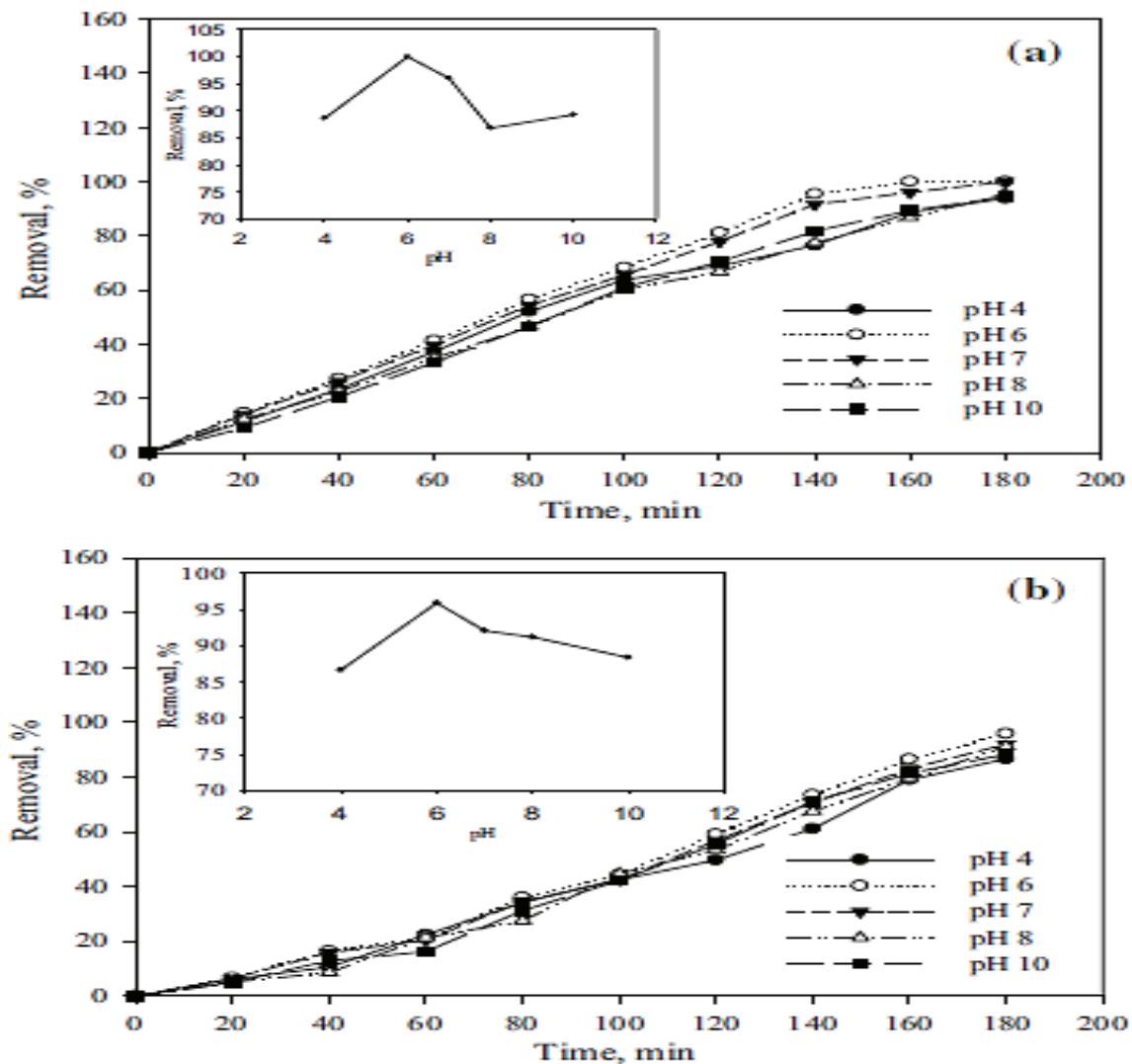


Fig. 7. The pH effects of methyl orange under the conditions of 200 mg L⁻¹ photocatalysts, and 10 mg L⁻¹ methyl orange on; (a) the rate of bleaching, (b) the rate of dye degradation

3.4. Photocatalyst dosage effects

To investigate the effects of photocatalyst dose on the bleaching and degradation of MO, a solution with a primary methyl orange concentration of 10 mg L⁻¹ and a reaction duration of 180 min was added to a range of photocatalyst doses from 100 to 500 mg L⁻¹. Figure 8 depicts the findings of these analyses. The result demonstrated that bleaching and degradation increased when the catalyst concentration was raised to 200 mg L⁻¹. When the catalyst concentration was increased to 400 mg L⁻¹, bleaching and degradation did not change noticeably, but when the catalyst

concentration was increased to 500 mg L⁻¹, bleaching and degradation decreased. As catalyst concentration grew, more surface active sites were available. As a result, there is an increase in the generation of hydroxyl radicals, which increases ZnO's photocatalytic activity. UV light cannot penetrate the catalyst's surface when the milky solution is in excess. As a result, these occurrences can reduce the generation of hydroxyl radicals, reducing the effectiveness of dye deterioration and solution pH discoloration [33,37]. For subsequent research, a dose of 200 mg L⁻¹ photocatalysts was used.

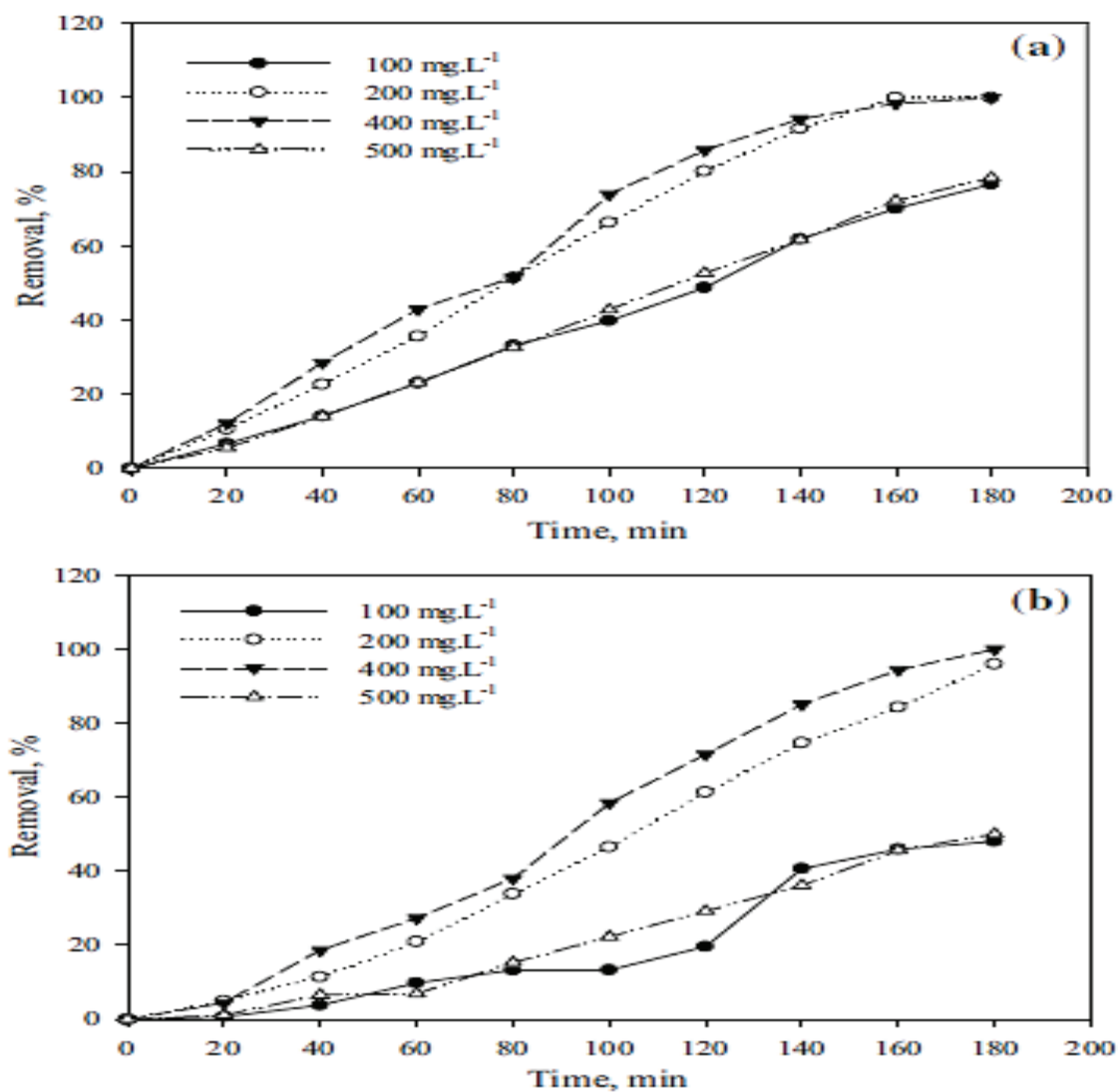


Fig. 8. Effect of catalyst amount of methyl orange under the conditions of pH 6, 180 minutes, and 10 mg L⁻¹ of methyl orange on; (a) the rate of bleaching (b) the rate of dye degradation

3.5. MO concentration effects

Several methyl orange (MO) concentrations (5-20 mg L⁻¹) at a reaction duration of 180 min and a primary pH of 6 were studied to ascertain the impact of primary MO concentration on the method's effectiveness. Figure 9 displays the outcomes of these analyses. The findings showed that raising the initial dye concentration reduced bleaching and degradation. This might be brought on by a decline in the number of active surface

sites. As a result, the generation of hydroxyl radicals declines, which may result in decreased photocatalytic activity. Furthermore, as the dye concentration increases, the distance of a photon into a dye solution shortens. To conduct additional research, MO at a concentration of 10 mg L⁻¹ was chosen because, at higher dye concentrations, the dye molecules may absorb more sunlight than the catalyst, which could reduce the catalyst's effectiveness [38, 39].

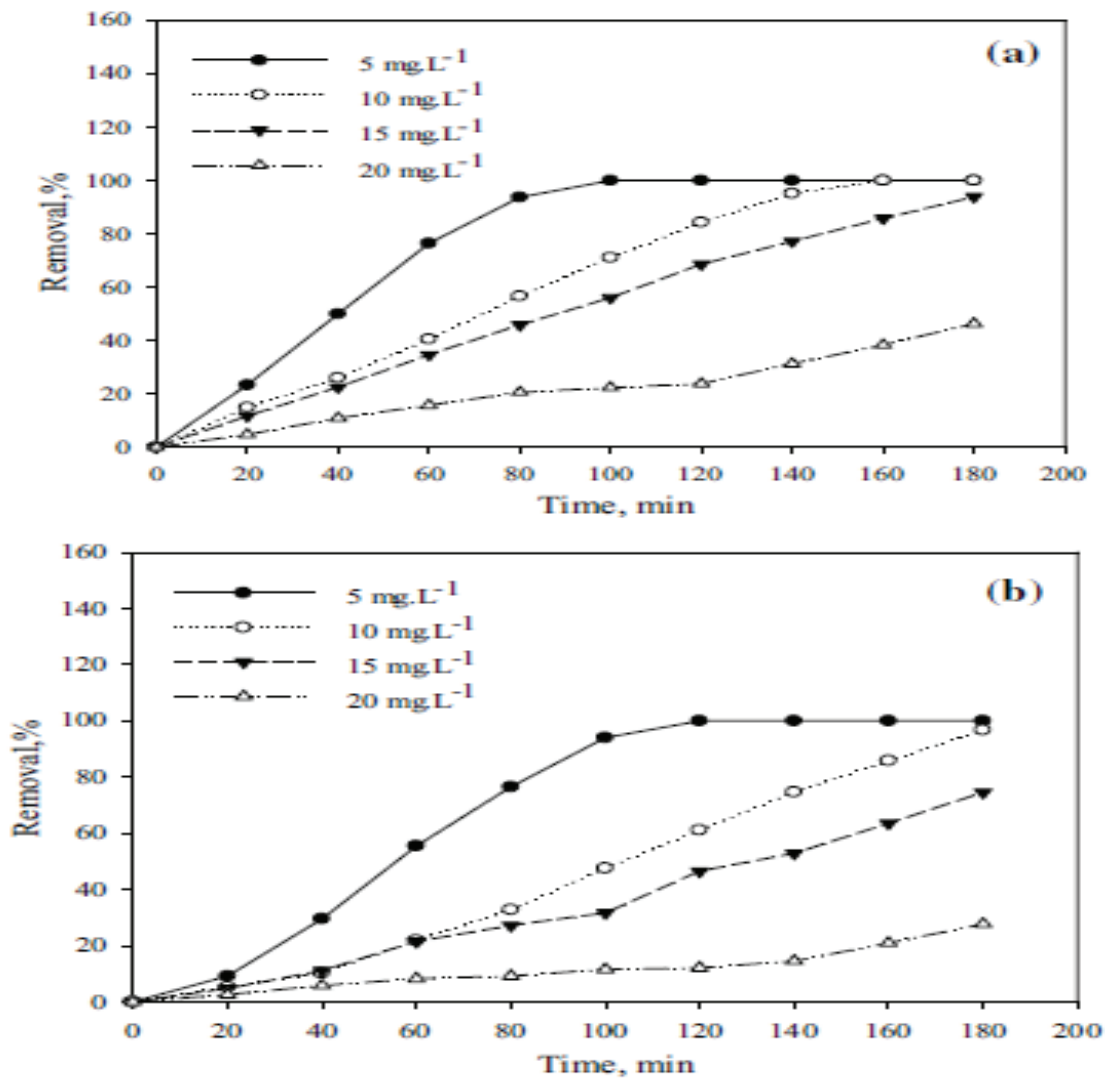


Fig. 9. Effect of primary concentration of MO under the conditions of pH 6, and 200 mg L⁻¹ photocatalysts on; (a) the rate of bleaching (b) the rate of dye degradation

3.6. Effects of stirring the mixture

To find out how stirring the solution affected the bleaching and degradation of MO, specific tests were conducted at reaction periods of 180 minutes, pH levels of 6, primary MO concentrations of 10 mg L⁻¹, and catalyst doses of 200 mg L⁻¹. Figure 10 percent (%) the findings of these analyses. The results show that swirling

the solution exacerbated the bleaching and deterioration. First, agitation causes turbulence in the solution, which promotes the solution's absorption of oxygen. In the synthesis of hydroxyl radicals, soluble oxygen is crucial. Second, stirring the solution shortens the time needed for equilibrium by accelerating MO transfer and surface diffusion [40].

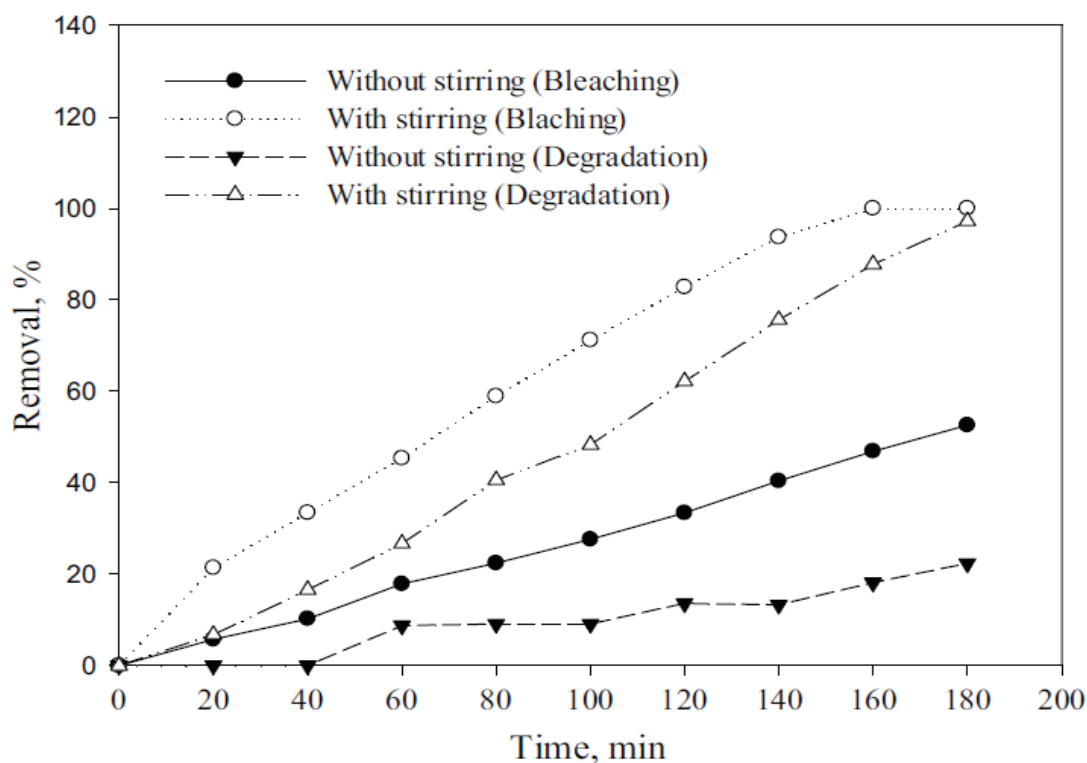


Fig. 10. Effect of solution stirring under the conditions of pH 6, 20 mg L⁻¹ photocatalysts, and 10 mg L⁻¹ methyl orange on the rate of bleaching and dye degradation

4. Conclusion

In the current work, methyl orange from aqueous solutions was subjected to a dye degradation process employing ZnO as a photocatalyst. The results showed that the AC-ZnO system successfully destroyed the MO dye. When ZnO was present, the rate of deterioration was high, but when ZnO wasn't there, the degradation rate decreased. The best dye degradation conditions were found at a pH of 6.0 with 200 mg L⁻¹ of photocatalyst for 10 mg L⁻¹ of MO based on agitating the dye solution in an air environment. The outcomes also demonstrated that synthetic photocatalysts in the actual world had much high efficacy and that recovering and reusing photocatalysts hurt the degradation rate and bleaching. The current study offered a novel, cost-effective adsorbent with great promise for treating wastewater contaminated with dyes.

5. Conflicts of interest

There are no conflicts to declare

6. Acknowledgements

This research is supported by the Physical Chemistry Lab., Chemist Department, College of Education for pure science (ibn-al Haitham), University of Baghdad.

7. References

- [1] C. Karthikeyan, P. Arunachalam, K. Ramachandran, A. M. Al-Mayouf, S. Karuppuchamy, Recent advances in semiconductor metal oxides with enhanced methods for solar photocatalytic applications, *J. Alloy Comp.*, 828 (2020) 154281. <https://doi.org/10.1016/j.jallcom.2020.154281>.

- [2] X. Nie, S. Wu, P. Lv, H. Ke, F. Huang, Q. Wei, Chameleon-inspired iridescent structural color textiles with reversible multiple stimulus-responsive functions, *Chem. Eng. J.*, 433 (2022) 134410. <https://doi.org/10.1016/j.cej.2021.134410>.
- [3] T. S. Naidu, C. M. Sheridan, L. D. van Dyk, Basic oxygen furnace slag: Review of current and potential uses, *Miner. Eng.*, 149 (2020) 106234. <https://doi.org/10.1016/j.mineng.2020.106234>.
- [4] F. M. Valadi, A. Ekramipooya, M. R. Gholami, Selective separation of Congo Red from a mixture of anionic and cationic dyes using magnetic-MOF: Experimental and DFT study, *J. Mol. Liq.*, 318(2020) 114051. <https://doi.org/10.1016/j.molliq.2020.114051>
- [5] K. Dahmani, D. E. Kherroub, A. Boucherdoud, B. Bestani, Removal of Ca (II) and Mg (II) hardness by ion exchange resins and soda ash for seawater pretreatment to reduce scale formation in evaporators multi-stage flash desalination, *Desalin. Water Treat.*, 221 (2021) 23-30. <https://doi.org/10.5004/dwt.2021.27020>.
- [6] X. Nie, S. Wu, P. Lv, H. Ke, F. Huang, Q. Wei, Chameleon-inspired iridescent structural color textiles with reversible multiple stimulus-responsive functions, *Chem. Eng. J.*, 433 (2022) 134410. <https://doi.org/10.1016/j.cej.2021.134410>.
- [7] N. Daneshvar, S. Aber, M. S. Dorraji, A. R. Khataee, M. H. Rasoulifard, Photocatalytic degradation of the insecticide diazinon in the presence of prepared nanocrystalline ZnO powders under irradiation of UV-C light, *Separ. Purif. Tech.*, 58 (2007) 91-98. <https://doi.org/10.1016/j.seppur.2007.07.016>.
- [8] D. F. Katowah, S. M. Saleh, S. A. Alqarni, R. Ali, G. I. Mohammed, M. A. Hussein, Network structure-based decorated CPA@CuO hybrid nanocomposite for methyl orange environmental remediation, *Sci. Rep.*, 11 (2021) 1-21. <https://doi.org/10.1038/s41598-021-84540-y>.
- [9] D. Vaya, P. K. Surolia, Semiconductor based photocatalytic degradation of pesticides: An overview, *Environ. Tech. Innovat.*, 20 (2020) 101128. <https://doi.org/10.1016/j.eti.2020.101128>.
- [10] A.R. Khataee, M.B. Kasiri, L. Alidokht, Application of response surface methodology in the optimization of photocatalytic removal of environmental pollutants using nanocatalysts, *Environ. Technol.*, 32(15) (2011) 1669-1684. <https://doi.org/10.1080/09593330.2011.597432>.
- [11] K. Jain, A. S. Patel, V. P. Pardhi, S. J. S. Flora, Nanotechnology in wastewater management: a new paradigm towards wastewater treatment, *Molecules*, 26 (2021) 1797. <https://doi.org/10.3390/molecules26061797>.
- [12] M. Amini, M. Kamkar, F. Rahmani, A. Ghaffarkhah, F. Ahmadijokani, M. Arjmand, Multilayer structures of a ZnO. 5NiO. 5Fe₂O₄-reduced graphene oxide/PVDF nanocomposite for tunable and highly efficient microwave absorbers, *ACS Appl. Elect. Mater.*, 3 (2021) 5514-5527. <https://doi.org/10.1021/acsaelm.1c00940>.
- [13] L. A. Goulart, G. O. Santos, K. I. Eguiluz, G. R. Salazar-Banda, M. R. Lanza, C. Saez, M. A. Rodrigo, Towards a higher photostability of ZnO photo-electrocatalysts in the degradation of organics by using MMO substrates, *Chemosphere*, 271 (2021) 129451. <https://doi.org/10.1016/j.chemosphere.2020.129451>.
- [14] S. Zhong, D. Xiong, B. Zhang, X. Yang, T. Yang, G. Tian, H. Zhang, W. Yang, W. Deng, Structurally unraveling the photocarrier behavior of Cu₂O/ZnO heterojunction photodetectors, *ACS Photo.*, 9 (2022) 268-274. <https://doi.org/10.1021/acsp Photonics.1c01490>.
- [15] M. Zare, K. Namratha, S. Alghamdi, Y. H. E. Mohammad, A. Hezam, M. Zare, Q. A. Drmosh, K. Byrappa, B. N. Chandrashekar, S. Ramakrishna, X. Zhang, Novel green biomimetic approach for synthesis of ZnO-Ag

- nanocomposite; antimicrobial activity against food-borne pathogen, biocompatibility and solar photocatalysis, *Sci. Rep.*, 9 (2019)1-15. <https://doi.org/10.1038/s41598-019-44309-w>.
- [16] P. K. Aspoukeh, A. A. Barzinjy, S. M. Hamad, Synthesis, properties and uses of ZnO nanorods: a mini review, *Int. Nano Lett.*, (2021)1-16. <https://doi.org/10.1007/s40089-021-00349-7>.
- [17] M. A. Desai, A. N. Vyas, G. D. Saratale, S. D. Sartale, Zinc oxide superstructures: recent synthesis approaches and application for hydrogen production via photoelectrochemical water splitting, *Int. J. Hydrogen Energ.*, 44 (2019) 2091-2127. <https://doi.org/10.1016/j.ijhydene.2018.08.042>.
- [18] M. Qamar, S. A. Zaidi, M. Rafatullah, M. Qutob, S. J. Kim, Q. A. Drmosh, Role of post-hydrothermal treatment on the microstructures and photocatalytic activity of TiO₂-based nanotubes, *Catalysts*, 12 (2022) 702. <https://doi.org/10.3390/catal12070702>.
- [19] S. Mishra, P. Supraja, P. R. Sankar, R. R. Kumar, K. Prakash, D. Haranath, Controlled synthesis of luminescent ZnS nanosheets with high piezoelectric performance for designing mechanical energy harvesting device, *Mater. Chem. Phys.*, 277 (2022) 125264. <https://doi.org/10.1016/j.matchemphys.2021.125264>.
- [20] A. Czyżowska, A. Barbasz, A review: zinc oxide nanoparticles—friends or enemies?, *Int. J. Environ. Health Res.*, 32 (2022) 885-901. <https://doi.org/10.1080/09603123.2020.1805415>.
- [21] M. S. Nasrollahzadeh, M. Hadavifar, S. S. Ghasemi, M. Arab Chamjangali, Synthesis of ZnO nanostructure using activated carbon for photocatalytic degradation of methyl orange from aqueous solutions, *Appl. Water Sci.*, 8 (2018) 1-12. <https://doi.org/10.1007/s13201-018-0750-6>.
- [22] B. Yulianto, L. Nulhakim, M. F. Ramadhani, M. Iqbal, A. Nuruddin, Improved performances of ethanol sensor fabricated on Al-doped ZnO nanosheet thin films, *IEEE Sens. J.*, 15 (2015) 4114-4120. <https://doi.org/10.1109/JSEN.2015.2410995>.
- [23] B. Ghanbarzadeh, S. A. Oleyaei, H. Almasi, Nanostructured materials utilized in biopolymer-based plastics for food packaging applications, *Crit. Rev. Food Sci. Nutr.*, 55 (2015) 1699-1723. <https://doi.org/10.1080/10408398.2012.731023>.
- [24] Z. Abid, A. Abbas, A. Mahmood, N. F. Rana, S. J. Khan, L. Duclaux, K. M. Deen, N. M. Ahmad, Water treatment using high performance antifouling ultrafiltration polyether sulfone membranes incorporated with activated carbon, *Polymers*, 14 (2022) 2264. <https://doi.org/10.3390/polym14112264>.
- [25] C. F. Holder, R. E. Schaak, Tutorial on powder X-ray diffraction for characterizing nanoscale materials, *ACS Nano*, 13 (2019) 7359-7365. <https://doi.org/10.1021/acsnano.9b05157>.
- [26] A. A. KHAMIS, A comparison of recent analytical methods for analysis of arsenic, *The Libyan Conference on Chemistry and Its Applications (LCCA)*, 1 (2021) 17-24. <http://repository.uob.edu.ly/handle/123456789/1617>.
- [27] F. Nekouei, H. Noorzadeh, S. Nekouei, M. Asif, I. Tyagi, S. Agarwal, V. K. Gupta, Removal of malachite green from aqueous solutions by cuprous iodide–cupric oxide nano-composite loaded on activated carbon as a new sorbent for solid phase extraction: isotherm, kinetics and thermodynamic studies, *J. Mol. Liq.*, 213 (2016) 360-368. <https://doi.org/10.1016/j.molliq.2015.07.058>.
- [28] T. Li, X. Ren, L. Bao, M. Wang, W. Bao, L. Chang, Effect of lignite as support precursor on deep desulfurization performance of semicoke supported zinc oxide sorbent in hot coal gas, *RSC Adv.*, 10 (2020) 12780-12787. <https://doi.org/10.1039/C9RA10884J>.
- [29] M. R. Al-Mamun, S. Kader, M. S. Islam, M. Z. H. Khan, Photocatalytic activity improvement and application of UV-TiO₂ photocatalysis

- in textile wastewater treatment: A review, *J. Environ. Chem. Eng.*, 7 (2019) 103248. <https://doi.org/10.1016/j.jece.2019.103248>.
- [30] P. Muthirulan, M. Meenakshisundaram, N. Kannan, Beneficial role of ZnO photocatalyst supported with porous activated carbon for the mineralization of alizarin cyanin green dye in aqueous solution, *J. Adv. Res.*, 4 (2013) 479-484. <https://doi.org/10.1016/j.jare.2012.08.005>.
- [31] F. Nekouei, H. Noorizadeh, S. Nekouei, M. Asif, I. Tyagi, S. Agarwal, V. K. Gupta, Removal of malachite green from aqueous solutions by cuprous iodide–cupric oxide nano-composite loaded on activated carbon as a new sorbent for solid phase extraction: isotherm, kinetics and thermodynamic studies, *J. Mol. Liq.*, 213 (2016) 360-368. <https://doi.org/10.1016/j.molliq.2015.07.058>.
- [32] Z. Noorimotlagh, R. Darvishi Cheshmeh Soltani, G. Shams Khorramabadi, H. Godini, M. Almasian, Performance of wastewater sludge modified with zinc oxide nanoparticles in the removal of methylene blue from aqueous solutions, *Des. Water Treat.*, 57 (2016) 1684-1692. <https://doi.org/10.1080/19443994.2014.977954>.
- [33] K. Bisaria, S. Sinha, R. Singh, H. M. Iqbal, Recent advances in structural modifications of photo-catalysts for organic pollutants degradation—a comprehensive review, *Chemosphere*, 284 (2021) 131263. <https://doi.org/10.1016/j.chemosphere.2021.131263>.
- [34] S. M. Saleh, ZnO nanospheres based simple hydrothermal route for photocatalytic degradation of azo dye, *Spectrochim. Acta Mol. Biomol. Spectros.*, 211 (2019) 141-147. <https://doi.org/10.1016/j.saa.2018.11.065>.
- [35] M. A. Hassaan, A. Pantaleo, L. Tedone, M. R. Elkatory, R. M. Ali, A. E. Nembr, G. D. Mastro, Enhancement of biogas production via green ZnO nanoparticles: Experimental results of selected herbaceous crops, *Chem. Eng. Comm.*, 208 (2021) 242-255. <https://doi.org/10.1080/00986445.2019.1705797>.
- [36] J. Saini, V. K. Garg, R. K. Gupta, N. Kataria, Removal of Orange G and Rhodamine B dyes from aqueous system using hydrothermally synthesized zinc oxide loaded activated carbon (ZnO-AC), *J. Environ. Chem. Eng.*, 5 (2017) 884-892. <https://doi.org/10.1016/j.jece.2017.01.012>.
- [37] V. I. Parvulescu, F. Epron, H. Garcia, P. Granger, Recent progress and prospects in catalytic water treatment, *Chem. Rev.*, 122 (2021) 2981-3121. <https://doi.org/10.1021/acs.chemrev.1c00527>.
- [38] S. G. Kumar, K. K. Rao, Zinc oxide based photocatalysis: tailoring surface-bulk structure and related interfacial charge carrier dynamics for better environmental applications, *RSC Adv.*, 5 (2015) 3306-3351. <https://doi.org/10.1039/C4RA13299H>.
- [39] N. Sobana, B. Krishnakumar, M. Swaminathan, Synergism and effect of operational parameters on solar photocatalytic degradation of an azo dye (Direct Yellow 4) using activated carbon-loaded zinc oxide, *Mater. Sci. Semicond. Process.*, 16 (2013) 1046-1051. <https://doi.org/10.1016/j.mssp.2013.01.002>.
- [40] M. Ghaedi, G. Negintaji, F. Marahel, Solid phase extraction and removal of brilliant green dye on zinc oxide nanoparticles loaded on activated carbon: new kinetic model and thermodynamic evaluation, *J. Ind. Eng. Chem.*, 20 (2014) 1444-1452. <https://doi.org/10.1016/j.jiec.2013.07.030>.